Journal of Alloys and Compounds 509 (2011) 4445–4451

Contents lists available at ScienceDirect

Journal of Alloys and Compounds

journal homepage: www.elsevier.com/locate/jallcom

Luminescence properties of lanthanide doped alkaline earth chlorides under (V)UV and X-ray excitation

Aleksander Zych*, Anke Leferink op Reinink, Koen van der Eerden, Celso de Mello Donegá, Andries Meijerink

CMI, Debye Institute for NanoMaterials Science, Utrecht University, Princetonplein 1, 3508TA Utrecht, The Netherlands

ARTICLE INFO

Article history:
Received 10 November 2010
Received in revised form 14 January 2011
Accepted 19 January 2011
Available online 26 January 2011

Keywords:
Rare earth alloys and compounds
Synchrotron radiation
Luminescence
Insulators

ABSTRACT

The photoluminescence and radioluminescence of Ce^{3+}, Pr^{3+} and Nd^{3+} in $SrCl_2$ and $BaCl_2$ are reported and discussed in relation to application as a (fast) scintillator material. The Ce^{3+} doped materials exhibit the typical fast cerium *d–f* emission (358, 382 nm in $SrCl_2$ and 350, 375 nm in $BaCl_2$) both under synchrotron and ionizing radiation excitations. A weak afterglow is observed. For Pr^{3+} a very fast *d–f* emission is observed in $SrCl_2$ (250, 263, 300 and 328 nm, $\tau = 13$ ns) and $BaCl_2$ (260, 288 and 315 nm, $\tau = 10$ ns), but only under direct *f–d* excitation. No *d–f* luminescence is observed for Pr^{3+} under X-ray excitation. The absence of *d–f* emission is explained by the energy of the host lattice emission which is too low for energy transfer to the high energy *fd* states of Pr^{3+} (230 nm in $SrCl_2$ and 235 nm in $BaCl_2$). The neodymium doped chlorides do not show *d–f* luminescence.

1. Introduction

Inorganic materials doped with lanthanide ions are well-known for their efficient luminescence related to the unique optical properties of the lanthanides originating from the partially filled 4*f* shell. As a result, lanthanide doped materials are widely used in applications where efficient emission of light is required, for example in lighting (fluorescent tubes, white light LEDs), displays and medical imaging. In the field of medical imaging there has been great interest in the past decades in the development of new scintillation materials for the conversion of high energy X-rays or gamma-rays into light. Mostly, scintillators are inorganic crystalline materials (e.g. halides, oxides, silicates, aluminates, tungstates), which emit short flashes of light in the UV–vis spectral range upon high energy radiation or particle irradiation. There are some stoichiometric scintillators known but most scintillators rely on emission from luminescent ions (activators) doped into the host lattice. The high energy radiation is deposited in the host lattice where it leads to the creation of electron–hole (e–h) pairs which recombine on or nearby the activator ion giving rise to efficient emission from the activator. Scintillators are of increasing interest due to a rise in the need for high energy radiation detectors, e.g. in high energy physics, space exploration, home land security and medical imaging. In the field of medical imaging scintillators are applied in positron emission tomography (PET), computed tomography (CT) and other X-ray imaging techniques and single photon emission computed tomography (SPECT). In the more advanced medical imaging techniques (PET, CT) better scintillators will lead to an increase in the precision of measurements to diagnose cancer earlier and to pinpoint the location of the tumor tissue in the patient's body, as well as decrease the exposure of the patients to the harmful ionizing radiation used in these examinations. The price of the scintillator materials used in these medical imaging machines is an important factor. PET is the technique with the most demanding requirements on the scintillators [1,2]. The emission must not only be efficient (preferably the scintillator material should generate at least 20,000 photons/MeV of incoming radiation) but also very fast, with the emission lifetime shorter than 40 ns, since the technique relies on the co-incident detection of gamma-rays emitted at an angle of 180° upon positron–electron annihilation.

Efficient and fast emission is achieved by incorporation of trivalent Ce^{3+} ions ($4f^1$) in an inorganic host lattice. The $5d–4f$ ($d–f$) emission of Ce^{3+} is due to fully allowed (parity and spin) transition with a typical radiative lifetime of 25–70 ns. A wide variety of Ce^{3+} doped materials has been investigated for application in PET scanners. At the same time, it has been realized that an even faster response leads to a better timing resolution and better discrimination between random and real events, giving a higher spatial resolution. New materials with faster response time can use the *d–f* emission of Pr^{3+} ($4f^2$) or Nd^{3+} ($4f^3$). The *d–f* emission from Pr^{3+} and Nd^{3+} is at higher energies which leads to faster radiative decay based on Fermi's golden rule [3,4].

Here we report the spectroscopic properties of Ce^{3+}, Pr^{3+} and Nd^{3+} in chloride host lattices. The choice for a chloride

* Corresponding author. Tel.: +31 30 2532203; fax: +31 30 2532403.
E-mail addresses: a.k.zych@uu.nl, alek_zych@yahoo.com (A. Zych).

0925-8388/$ – see front matter © 2011 Elsevier B.V. All rights reserved.
doi:10.1016/j.jallcom.2011.01.120

host is motivated by the recently reported high photon yields (>80,000 photons/MeV) for Ce^{3+} in LnX_3 (Ln = La, Lu; X = Cl, Br, I) [5–8]. Possibly, incorporation of Pr^{3+} in a chloride host leads to a combination of a faster decay and high photon yield. Alkaline earth halides are known to show fast emission when doped with trivalent cerium ions [9–16]. Previous work on Ce^{3+} doped into alkaline earth chlorides has revealed Ce^{3+} *d–f* emission around 360 nm and 390 nm ($SrCl_2$) and 350 nm and 375 nm ($BaCl_2$), while the lowest *f–d* excitation bands are observed around 320 nm and 335 nm in strontium and barium chlorides, respectively [10–16]. No reports have been found in the literature on the luminescence of Pr^{3+} and Nd^{3+} in $SrCl_2$ or $BaCl_2$. Here we will show that Pr^{3+} shows fast *d–f* emission in both $SrCl_2$ and $BaCl_2$. Use of the materials as scintillators is however hampered by the absence of energy transfer from the host lattice to the emitting *fd* state.

2. Experimental

2.1. Synthesis and characterization

The materials were synthesized by melting and rapid quenching of the starting materials (anhydrous chlorides) in a glassy carbon crucible in a high frequency furnace, similar to the method reported earlier for sodium chloride [17]. This allows for fast synthesis of simple chemical compositions even in the case of ionic radii and charge mismatch between the dopant and the host lattice cations. The samples obtained are polycrystalline. The mixture of anhydrous chlorides was dried over night at 200 °C under a constant nitrogen flow. Then the temperature was raised to 300 °C and maintained as such for 2 h. Subsequently, melting at about 1000 °C ($SrCl_2$) or 1100 °C ($BaCl_2$) took place and after 15 min the melt was rapidly quenched to room temperature. The samples showed uniform red luminescence (in case of praseodymium doped host lattices) when observed under UV excitation (254 nm).

The crystal structure of the samples was checked by X-ray powder diffraction (XRD), using a PW 1729 Philips diffractometer, equipped in a Cu K_α X-ray source (λ = 1.5418 Å). The XRD patterns of the compounds synthesized have been compared with the theoretical patterns of strontium chloride [18] and barium chloride [19]. Strontium chloride can exist in several different crystal structures. The compounds that have been synthesized are cubic ($a = b = c = 6.98$ Å and $\alpha = \beta = \gamma = 90°$), with a density of 3.09 g/cm^3. Barium chloride can also crystallize in various crystal structures depending on the synthesis conditions. The samples that were obtained were orthorhombic ($a = 7.88$ Å, $b = 9.42$ Å, $c = 4.73$ Å and $\alpha = \beta = \gamma = 90°$), with a density of 3.94 g/cm^3. The strontium chloride materials show some additional peaks in the XRD patterns. This is attributed to the hygroscopicity of the material, which results in structural change due to incorporation of water and creation of different hydrates of strontium chloride, possibly during the collection of the XRD pattern.

2.2. Optical measurements

Luminescence spectra have been measured using synchrotron radiation at SUPERLUMI station (DESY, Hamburg) which is an excellent station for vacuum UV (VUV) spectroscopy. A more elaborate description of the set-up can be found elsewhere [20]. In short, the VUV part of the synchrotron spectrum is dispersed in an excitation monochromator giving the option to measure high resolution excitation spectra between ~65 and 335 nm, with a 0.3 nm resolution. Emission can be coupled into different monochromator/detector combinations, allowing for the measurement of emission between 120 and 1000 nm. The synchrotron spectra have been measured in three time windows (integrated, fast and slow) making it possible to distinguish between fast and slow emissions. Luminescence lifetimes have been recorded with a timing resolution of about 200 ps using time-to-amplitude conversion (TAC). The excitation spectra have been corrected for signal intensity distribution with a spectrum of sodium salicylate. The emission spectra were not corrected for detector response. The samples have been placed in a cold finger cryostat on a copper sample holder.

Emission measurements under soft-X-ray excitation (radioluminescence) have been carried out at room temperature, using the white spectrum of a copper tube operated at 40 kV, with the energy in the maximum of the white band of about 28.7 keV. Afterglow of the investigated materials has been measured as well, using the same set-up.

Due to the hygroscopic character of the materials investigated, special care was taken to prevent incorporation of water. The samples were stored in sealed plastic bags that were UV transparent. Additionally, the samples have been stored in a desiccator above dry silica beads. Only in case of XRD and synchrotron measurements the samples were taken out of the protective bags. The XRD patterns were recorded under ambient conditions which can explain the observation of small lines related to hydrated phases in some cases.

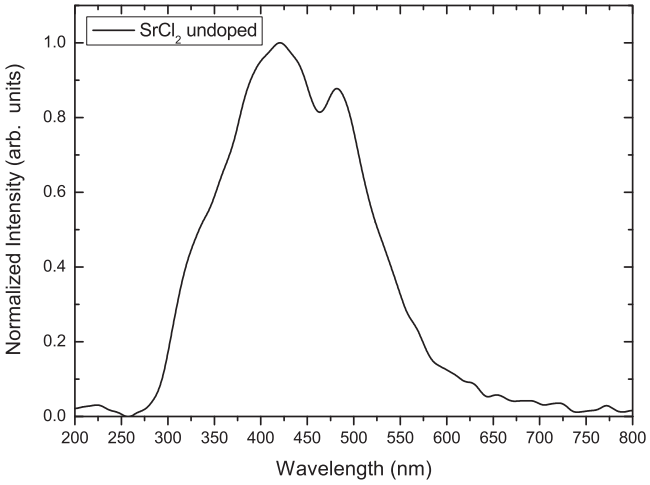

Fig. 1. Emission spectrum of undoped $SrCl_2$ under X-ray irradiation (26.7 keV), at 300 K.

3. Results and discussion

3.1. Luminescence spectroscopy

3.1.1. Undoped $SrCl_2$ and $BaCl_2$

The bandgaps reported in the literature for $SrCl_2$ and $BaCl_2$ differ slightly and have been estimated to be 7.5 eV (165 nm) and 7.0 eV (177 nm) for strontium chloride and barium chloride, respectively [21]. The estimate is only approximate, since the bandgap depends on the crystal structure, which has not been mentioned in the cited reference [21]. The luminescence of the undoped barium chloride has been extensively studied in the past [22,23]. Two major emission bands are observed with maxima at around 310 nm and 450 nm. The former has been ascribed to the STE emission and occurs only under excitation in the excitonic absorption peak [22], while the latter has been assigned to the F-V_k center recombination [23]. However, no reports on the spectroscopic properties of the undoped $SrCl_2$ host lattice have been found in the literature. In Fig. 1 a typical spectrum of the undoped $SrCl_2$ host lattice under X-ray excitation is presented. Two major emission bands are observed, peaking at around 420 nm and 483 nm. There is an additional small intensity band present around 225 nm and a shoulder to the main emission band at 420 nm, which is located at around 328 nm. The exact origin of these bands has not been investigated, though the small intensity band at around 225 nm might be an STE emission, while the main broad emission band at 420 nm could be related to the V_k center radiative recombination, analogues to that observed for $BaCl_2$. Since the crystal structure of both the materials is different, the observed features would be located at different wavelengths. The broadened peak at about 480 nm might also be a defect of some sort.

3.1.2. Ce^{3+} doped $SrCl_2$ and $BaCl_2$

Strontium chloride has been doped with trivalent cerium ions and the luminescence spectra have been recorded under different excitation wavelengths. A typical emission spectrum is presented in Fig. 2. The black curve corresponds to the emission as observed under a 293 nm excitation. The emission spectrum shows two broad bands, located at about 358 and 382 nm. The bands are assigned to transitions from the lowest *fd* state of Ce^{3+} to the $^2F_{5/2}$ and $^2F_{7/2}$ $4f^1$ ground state of Ce^{3+}. The observed energy separation between the two bands is about 1755 cm^{-1}, which is close to the expected spin–orbit splitting of 2000 cm^{-1}. It should be noted that in case of strontium chloride the trivalent cerium ions enter the divalent host lattice site. Due to the need of charge compensation

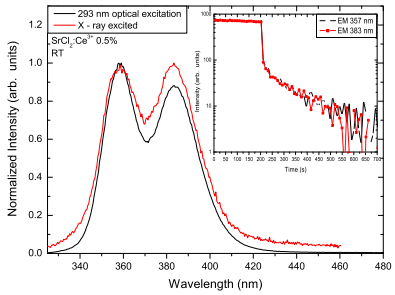

Fig. 2. Emission spectra of $SrCl_2$:Ce^{3+} 0.5% under UV excitation (293 nm, black line) and under X-ray irradiation (26.7 keV, red line), at 300 K. The inset shows the afterglow curves for the 357 nm and 383 nm emissions after X-ray irradiation. (For interpretation of the references to color in this figure legend, the reader is referred to the web version of the article.)

multiple lanthanide sites occur in the sample and can also give rise to different emission wavelengths.

The emission lifetime has been measured under direct *f–d* excitation at 325 nm, monitoring the 340 nm Ce^{3+} *d–f* emission (Fig. 3). For 0.1% Ce sample a decay time of 26 ns is measured at 300 K.

In $BaCl_2$ doped with Ce^{3+} the emission spectrum is similar to that for $SrCl_2$:Ce^{3+}. There is a slight blue shift of the emission bands, which are located around 350 and 375 nm for 295 nm excitation, as shown in Fig. 4 (black curve). The energy separation of the bands is about 1900 cm^{-1}, which corresponds well to the expected separation of 2000 cm^{-1}. Just as for $SrCl_2$, also for $BaCl_2$ differently charge compensated sites may influence the observed splitting in two bands. The results obtained for $BaCl_2$:Ce^{3+} are in line with earlier reports in the literature [10–13]. Further comparison with the literature data will follow in the section on radioluminescence. The emission lifetime has been measured under a direct *f–d* excitation at 275 nm for 350 nm emission (Fig. 5). A single exponential fit gives a decay time of 19 ns.

3.1.3. Pr^{3+} doped $SrCl_2$ and $BaCl_2$

Emission spectra were recorded for $SrCl_2$:Pr^{3+} under excitation at 165 nm (the excitonic absorption edge) and 236 nm (in the lowest energy *fd* band) at 8 K (Fig. 6). Under direct excitation in the *fd* band (Fig. 6A), four emission bands are observed, around 250, 263, 300 and 328 nm, as well as a very broad and low intensity band between 400 and 550 nm with maxima around 430, 460 and 490 nm. The broad band is assigned to a defect luminescence. Due to low resolution of the emission monochromator used, it is possible that the 490 nm maximum is in fact the $^3P_0 \rightarrow {}^3H_4$ transition on Pr^{3+}. The visible emission is stronger in the slow time window, indicating that the decay time is slower than ~100 ns. This is expected for

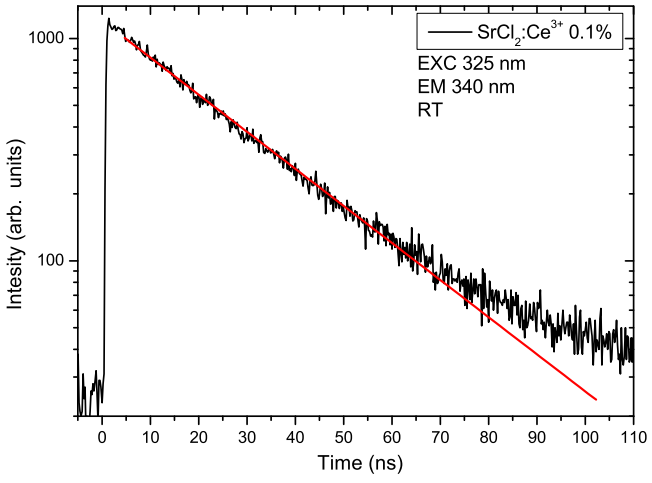

Fig. 3. Luminescence decay curve of the Ce^{3+} *d–f* emission (340 nm) in $SrCl_2$:Ce^{3+} 0.1% under direct excitation in the *fd* band (325 nm). The drawn line corresponds to a fit to single exponential decay with τ = 26 ns.

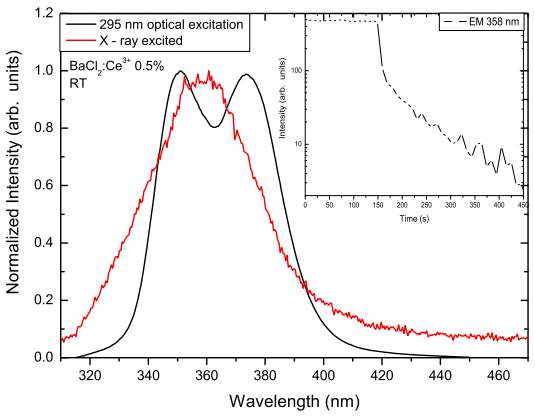

Fig. 4. Emission spectra of $BaCl_2$:Ce^{3+} 0.5% under UV excitation (295 nm, black line) and under X-ray irradiation (26.7 keV), at 300 K. The inset shows the afterglow curve for the 358 nm emission after X-ray irradiation. (For interpretation of the references to color in this figure legend, the reader is referred to the web version of the article.)

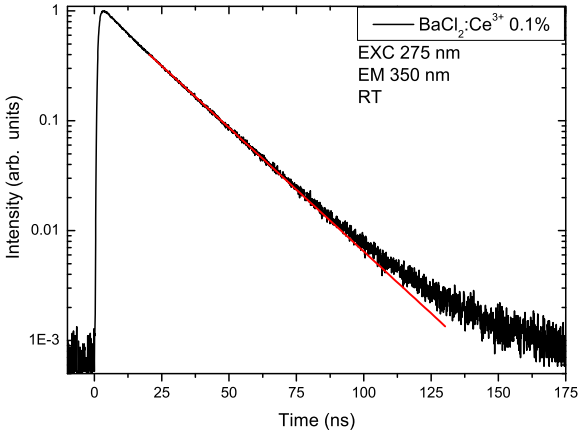

Fig. 5. Luminescence decay curve of the Ce^{3+} *d–f* emission (350 nm) in $BaCl_2$:Ce^{3+} 0.1% under direct excitation in the *fd* band (275 nm) at 8 K. The drawn line corresponds to a fit to single exponential decay with τ = 19 ns.

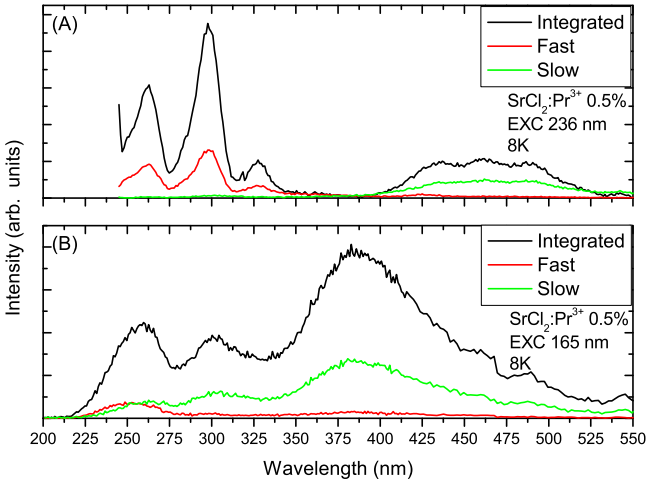

Fig. 6. Emission spectra of $SrCl_2$:Pr^{3+} 0.5% for excitation into the host lattice at 165 nm (A) and direct excitation into the *fd* band of Pr^{3+} at 236 nm (B). The spectra were recorded in different time windows (fast, slow and integrated, see also Section 2.2) at 8 K.

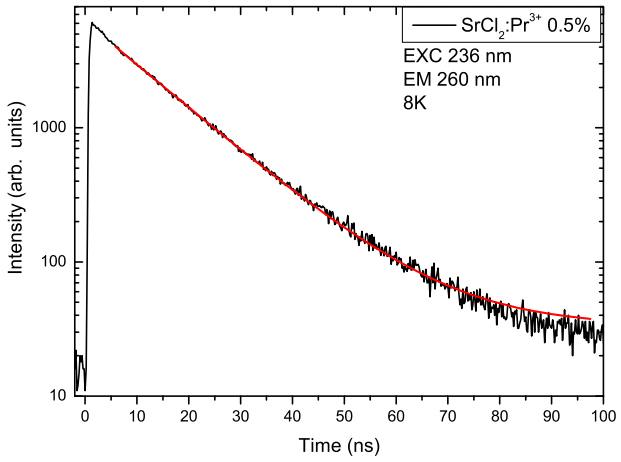

Fig. 7. Luminescence decay curve of the Pr^{3+} *d–f* emission (260 nm) in $SrCl_2$:Pr^{3+} 0.5% under direct excitation in the *fd* band (236 nm) at 8 K. The drawn line corresponds to a fit to single exponential decay with $\tau = 13$ ns.

defect-related emission at low temperatures. The emission bands in the UV part of the spectrum are stronger in the fast time window, indicating that these are the transitions from the lowest *f–d* state of Pr^{3+} which will have a fast (ns) decay time. The bands have been assigned to transitions from the lowest *fd* state to the $^3H_4$, $^3H_5$, $^3F_3$ and $^1G_4$ 4*f* states of Pr^{3+} for the bands located at 250, 263, 300 and 328 nm, respectively. The separation between the bands agrees well with the known energy differences between the $^3H_4$, $^3H_5$, $^3F_3$ and $^1G_4$ states.

Under excitonic excitation at 165 nm (Fig. 6B), the emission spectrum consists of three broad bands in the range 210 nm to about 550 nm. The maxima of the bands are located around 260 nm (with a small shoulder like feature at 237 nm), 300 nm and at 390 nm (with a tail extending to about 550 nm). The bands are stronger in the slow time window, indicating a long luminescence lifetime although some fast emission is observed between 240 and 320 nm. These UV emission bands may have a contribution from Pr^{3+} *d–f* emission. Feeding of the *fd* state through the excitonic state may also result in a longer lifetime for delayed *d–f* emission. The fact that the emission bands are broader than under direct excitation may be caused by broadening resulting from differently charge compensated Pr^{3+} sites, which are excited non-selectively under excitonic excitation. However, also defect related emission from the $SrCl_2$ host lattice has been observed in the spectral region around 300 nm. Due to the strong overlap it is hard to assign the UV emission bands to *d–f* or host lattice emissions. The strong emission band around 390 nm is assigned to defect emission. Its position is consistent with the bands observed in the emission spectrum of the undoped $SrCl_2$ host lattice under ionizing radiation excitation, presented in Fig. 1.

The lifetime of the praseodymium *d–f* emission in strontium chloride has been measured under a direct *f–d* excitation at 8 K for a sample activated with 0.5% Pr^{3+}. The decay curve is presented in Fig. 7. The decay is single exponential, with a decay time of 13 ns. This is much shorter than the decay times measured for Ce^{3+} emission and is promising for application as a scintillator material.

The emission spectra of Pr^{3+} in $BaCl_2$ (at 8 K) are shown in Fig. 8 for two different excitation wavelengths, 168 nm (excitonic) and 230 nm (*f–d* excitation). Under a direct *f–d* excitation the emission spectrum consists of two sets of emission bands as shown in Fig. 8A. The emissions in the UV part of the spectrum are located at around 260, 288 and 315 nm. These emission bands can be observed in the fast time window, indicating that they are related to the transitions from the lowest *fd* state to the $4f^2$ levels, $^3H_4$, $^3H_6$, $^3F_4$, respectively. The $fd \rightarrow {}^3H_5$ is not observed as a separate band, probably because it overlaps with the $fd \rightarrow {}^3H_4$ transition which is close in energy. It should be noted that the emission band that has been assigned to the $fd \rightarrow {}^3F_4$ transition overlaps with a slower decaying band around 310 nm. This indicates that there is an emission of different nature present at that wavelength that can also be excited at 230 nm, probably a host lattice related emission band. The emission bands between 350 nm and 500 nm are assigned to the defect related emissions. The small peak at 490 nm is probably $^3P_0 \rightarrow {}^3H_4$ emission of Pr^{3+}.

The emission spectrum of $BaCl_2$:Pr^{3+} 2% under excitonic excitation at 168 nm (Fig. 8B) shows a very broad band from about 240 to 600 nm, peaking at 390 nm. This band is assigned to the host lattice emission, as the one observed in the literature for $BaCl_2$ [22], similar to the band observed in $SrCl_2$. There is also a sharper spectral feature present at about 490 nm which is assigned to the $^3P_0 \rightarrow {}^3H_4$ emission. The presence of this emission demonstrates that there is energy transfer from the excitonic state to the 4*f* levels of praseodymium. However, no transition from the lowest *f–d* state has been observed in the region between 250 and 300 nm, contrary to observation for $SrCl_2$:Pr^{3+} where *d–f* emission from Pr^{3+} was observed after excitonic excitation, albeit weak. This indicates that there is no energy transfer from the host lattice excitonic state to the *fd* state of Pr^{3+} in $BaCl_2$:Pr^{3+}. An interesting spectral feature can be observed around 450 nm. The peculiar dip in the host lattice emission spectrum is a clear signature of radiative energy transfer to the praseodymium $^3P_2$ level. This will be followed by emission from the $^3P_0$ level to the $^3H_4$ ground state. In addition to radiative energy transfer there may also be non-radiative transfer. The praseodymium *d–f* emission lifetime in barium chloride has been measured at 8 K under a direct *fd* excitation for the 2% doped sample. The luminescence decay curve is shown in Fig. 9. The decay curve has a non-exponential initial part followed by a more exponential tail. The tail has been fit to a single exponential which results in a decay time of 10 ns. The non-exponential initial part can be explained by cross-relaxation quenching for neighboring Pr^{3+} ions. At 2% of Pr^{3+} it is known that cross-relaxation starts to depopulate the *fd* excited state. The tail represents the decay for isolated Pr^{3+} ions and the fit gives a reliable estimate of the radiative decay rate of the *fd* state. Some non-exponentiality may also be introduced by the presence of multiple sites with different local charge compensation. The 10 ns lifetime is among the shortest radiative lifetimes that have been reported for Pr^{3+} *d–f* emission. For example, the radiative lifetime for the *d–f* emission from Pr^{3+} in the

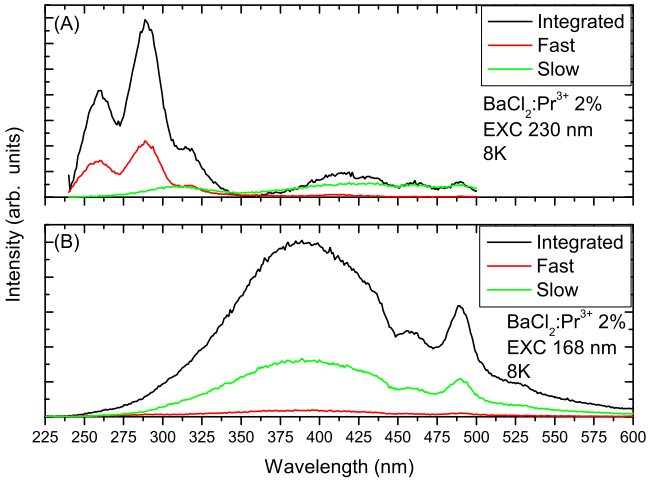

Fig. 8. Emission spectra of $BaCl_2$:Pr^{3+} 2% for excitation into the host lattice at 168 nm (A) and direct excitation into the *fd* band of Pr^{3+} at 230 nm (B). The spectra were recorded in different time windows (fast, slow and integrated, see also Section 2.2) at 8 K.

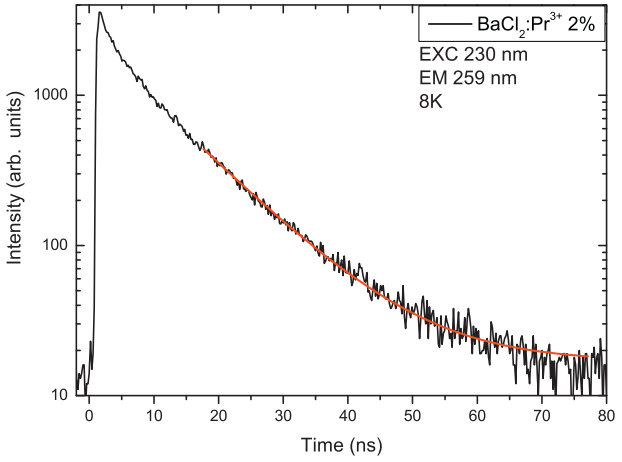

Fig. 9. Luminescence decay curve of the Pr^{3+} *d–f* emission (259 nm) in $BaCl_2$:Pr^{3+} 2% under direct excitation in the *fd* band (230 nm) at 8 K. The drawn line corresponds to a fit to single exponential decay for the tail of the curve with $\tau = 10$ ns.

scintillator material LuAG:Pr is 22 ns. The faster radiative decay rate in $BaCl_2$ is explained by the shorter emission wavelength (260 nm) and the higher refractive index of the material. The short decay time is favorable for application in PET scanners where a shorter radiative lifetime contributes to a better image quality.

3.1.4. Nd^{3+} doped $SrCl_2$ and $BaCl_2$

The lowest energy *fd* level for Nd^{3+} in $SrCl_2$ is expected to be located around 185 nm based on the position of the *fd* level for Ce^{3+} in $SrCl_2$ and the shift of 22,720 cm^{-1} to higher energy predicted by the Dorenbos relation [3]. The emission spectrum of neodymium doped strontium chloride only shows slow *f–f* emission, even when it is excited directly into the *fd* states (185 nm).

For $BaCl_2$:Nd^{3+} the lowest *fd* state of Nd^{3+} is expected around 189 nm. Just as for $SrCl_2$:Nd^{3+}, no *d–f* luminescence is observed, even under a direct *f–d* excitation. Instead, there is feeding of the $4f^3$ states of neodymium and only the slow intraconfigurational emission could be observed.

A possible explanation for the lack of Nd *d–f* emission in both $SrCl_2$ and $BaCl_2$ is that the lowest energy *fd* band of Nd in these host lattices is at higher energies than host lattice excited states, leading to energy transfer from *fd* states to defect states, which in turn populate high energy $4f^3$ neodymium levels through energy transfer. It also cannot be excluded that the *fd* states of Nd^{3+} are located close to or in the conduction band of $SrCl_2$ and $BaCl_2$. In this case excitation in the *f–d* state results in an impurity trapped exciton state that can relax by feeding the lower lying $4f^3$ levels of Nd^{3+}, leading to the slow *f–f* emission.

3.2. Radioluminescence

Radioluminescence is an important tool in the investigation of potential scintillator materials. It allows to study the luminescence properties under X-ray excitation. Under high energy excitation the efficiency of energy transfer from the host lattice to the activator ion can be investigated along with the kinetics. Also the radiation stability can be evaluated for excitation with ionizing radiation. Finally, it allows for an evaluation of the overall scintillation efficiency and of (undesired) afterglow properties.

3.2.1. Ce^{3+} doped $SrCl_2$ and $BaCl_2$

Under ionizing radiation the Ce^{3+} emission for $SrCl_2$:Ce consists of two broad bands that are consistent in shape and spectral location with the spectra observed under UV excitation (see Fig. 2, red curve). This proves that the emission comes from Ce^{3+} in $SrCl_2$. The bands are located at 360 nm and 384 nm. Upon ending X-ray excitation afterglow was present and it could be measured (for the 0.5% doped sample) for up to about 8 min after removal of the excitation source. The recorded afterglow decay is presented in the inset of Fig. 2. The afterglow is related to the slow release of trapped charge carriers generated under X-ray excitation. Recombination of thermally released charge carriers on or near the Ce^{3+} ions results in Ce^{3+} emission. Traps for free charge carriers may pre-exist in the material but the formation of traps can also be induced by the high energy irradiation.

A peculiar change in the relative intensities of the two Ce^{3+} emission bands was observed during irradiation. Both bands become weaker but the decrease in intensity of the longer wavelength band is much stronger. Probably this is due to the formation of color centers which absorb more strongly at the wavelength of the longer wavelength emission band. After prolonged irradiation the sample turns grayish indicating that color centers are formed.

The scintillation efficiency increased when the Ce^{3+} concentration was increased from 0.5% to 2%. The increase, based on the long wavelength band at 384 nm, is of about 40% for the 2% doped sample, compared to the 0.5% one. This is due to the larger number of Ce^{3+} ions available for excitation. By increasing the concentration of the activator ions, the probability of the excitation energy being captured by them increases. Otherwise the energy would have been lost through competing channels (e.g. recombination at trap sites).

Ce^{3+} emission in $BaCl_2$ has also been studied under ionizing radiation excitation. The emission spectrum consists of one broad band (red curve in Fig. 4), located around 358 nm. The position is similar to that observed under UV excitation but the characteristic doublet structure of Ce^{3+} emission has disappeared. The spectrum is also different from previous reports in the literature [10–13], where two emission bands have been observed under ionizing radiation excitation. Selling et al. have also observed a weak band around 300 nm that they have ascribed to the STE emission in barium chloride [12,23]. No such emission has been observed in the present study. The reasons for such a discrepancy are not clear. The single broad emission band around 358 nm has been observed for all samples, with Ce^{3+} concentrations of 0.1%, 0.5% and 2%. The origin of the change in the emission spectrum may be radiation induced defects. The softer $BaCl_2$ is more prone to the creation of defects than $SrCl_2$. Due to defect formation, the local environment of the Ce^{3+} ions changes and the disorder causes broadening of the Ce^{3+} emission bands, and therefore the 2000 cm^{-1} splitting can no longer be observed. This observation is in contrast to the results presented by Selling et al. [12], although it should be pointed out that in the cited reference the authors have used a different excitation source for X-rays. It is possible that the dose of the radiation was different in their case, which would lead to the observed difference, but this aspect has not been further investigated.

The afterglow of the Ce^{3+} emission in $BaCl_2$ under X-ray excitation has been measured for the 0.5% doped sample. The emission could be detected for up to 6 min after the excitation has been stopped. The resulting afterglow decay is presented in the inset of Fig. 4. Just as in case of $SrCl_2$:Ce^{3+} the afterglow is assigned to the slow thermally activated release of trapped charge carriers.

The highest scintillation intensity has been observed for the 2% doped sample and the intensity has increased in the concentration series from 0.1% to 2%. The increase when going from the 0.1% doped sample to the 0.5% doped one is of about 18%. When the concentration has been increased to 2%, the increase in the scintillation efficiency compared to the 0.1% doped sample has been about 62%. Just as in the case of $SrCl_2$:Ce^{3+} this observation is explained in the terms of a greater number of activator ions available for excitation by the created electron–hole pairs (which number for a specific material and specific excitation is constant), leading to

the increased probability that the excitation energy will reach the activators, leading to increased luminescence intensity.

3.2.2. Pr^{3+} doped $SrCl_2$ and $BaCl_2$

To investigate the efficiency of the fast *d–f* emission of Pr^{3+} under X-ray excitation, the emission spectrum of $SrCl_2$:Pr^{3+} (0.5% and 2%) has been measured under X-ray excitation and is shown in Fig. 10. The spectrum consists of a broad band around 400 nm and two sets of sharp emission lines at about 490 nm and 600–650 nm. The broad band emission is consistent with the previously observed host lattice emission of $SrCl_2$. The sharp lines are assigned to the Pr^{3+} *f–f* emission. No Pr^{3+} *d–f* emission is observed. This indicates that the energy transfer from the electron-hole pairs created by the X-rays to the *fd* state of Pr^{3+} is inefficient. This is consistent with the VUV luminescence measurement discussed in the previous section. The host lattice emission is too low in energy and there is no spectral overlap with the *f–d* excitation bands of Pr^{3+}, which are situated at high energies. There is spectral overlap with the $4f^2$ excitation lines and as a result, there is partial energy transfer to the $4f^2$ levels (^3P_J) of Pr^{3+}, resulting in the *f–f* emission lines. The presence of host lattice emission in the spectrum of the 0.5% doped sample shows that at this dopant concentration there is only partial energy transfer from the host lattice to Pr^{3+}. To increase the energy transfer efficiency the Pr^{3+} concentration has been increased to 2%. This strongly reduces host lattice emission intensity, showing that the energy transfer from the host lattice is indeed more efficient, but also the Pr^{3+} emission intensity decreases by a factor of about 7. This is explained by the cross-relaxation quenching of the Pr^{3+} emission, which is well known to occur at higher Pr concentrations and starts at Pr^{3+} concentrations as low as 0.5%.

The Pr^{3+} emission in $BaCl_2$ under ionizing radiation excitation has been investigated by measuring the X-ray excited emission spectra for three samples with Pr^{3+} concentrations of 0.1%, 0.5% and 2%. The spectrum of the 0.5% doped sample is presented in Fig. 11 and shows line emission between 490–550 nm and 600–725 nm due to Pr^{3+} *f–f* emission. Just as for $SrCl_2$:Pr, no *d–f* emission is observed showing that there is only energy transfer from the host lattice excited states to the $4f^2$ states of Pr^{3+} and not to the *fd* states. A very low intensity band is observed around 325 nm. It is most likely that this weak emission band is STE emission in $BaCl_2$, since its position is consistent with the one reported by Selling et al. [10]. There is only very weak host lattice emission in the sample with 0.5% Pr. The emission spectrum of the 0.1% doped $BaCl_2$ sample (not shown) does show a strong host lattice emission band around

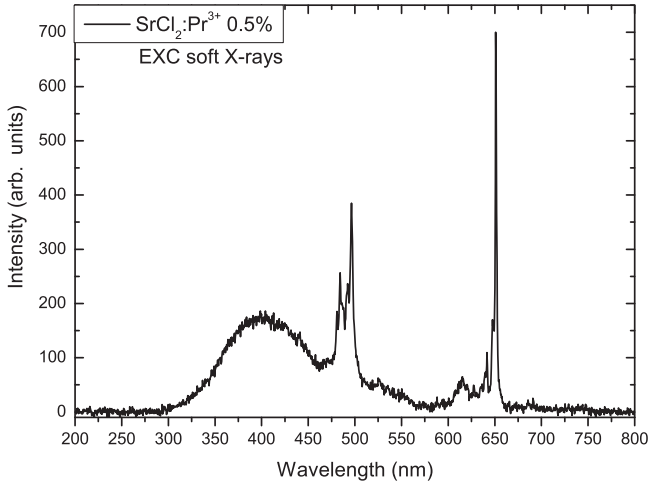

Fig. 10. Emission spectrum of $SrCl_2$:Pr^{3+} 0.5% at 300 K under X-ray excitation (Cu-source, operated at 40 kV).

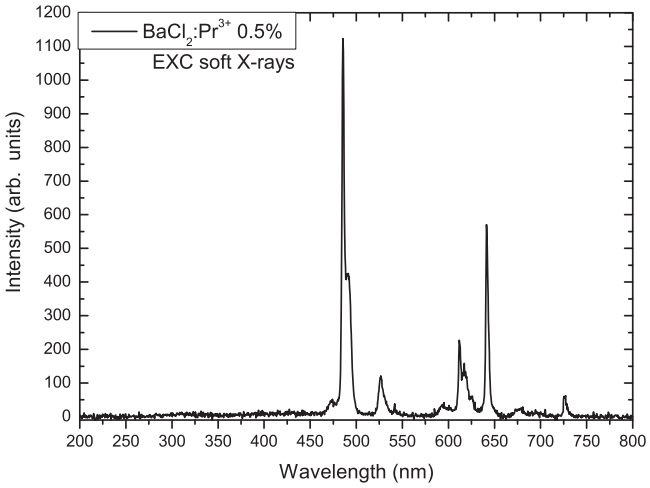

Fig. 11. Emission spectrum of $BaCl_2$:Pr^{3+} 0.5% at 300 K under X-ray excitation (Cu-source, operated at 40 kV) at 300 K.

435 nm. When the Pr content is increased to 2%, the emission spectrum under X-ray irradiation is very similar to the one of the 0.5% doped material. The faint broad band emission is still present alongside the sharp line emissions of Pr^{3+}. There is a decrease in the intensity of the praseodymium emission as compared to the 0.5% doped sample (~factor 1.6) due to cross-relaxation at the high Pr concentrations. The absence of *d–f* emission in $BaCl_2$ under excitation with X-rays is, just as for $SrCl_2$:Pr, due to the lack of spectral overlap between the emission of the host lattice and the absorption of the Pr *fd* states which are situated at too high energies.

Comparison of the luminescence from $SrCl_2$:Pr and $BaCl_2$:Pr shows that the energy transfer from the host lattice to the Pr^{3+} $4f^2$ states is more efficient in $BaCl_2$:Pr, leading to stronger Pr^{3+} emission in $BaCl_2$ under X-ray excitation. Secondly, the intensity ratio between the green $^3P_0 \rightarrow {}^3H_4$ (around 500 nm) and red $^3P_0 \rightarrow {}^3F_J$ (around 600–650 nm) 4*f* emission is reversed for the two materials.

4. Conclusions

$SrCl_2$ and $BaCl_2$ host lattices have been doped with Ce^{3+}, Pr^{3+} and Nd^{3+} to investigate the luminescence properties of the fast *d–f* emission and the potential for application as a fast scintillation material. Efficient and fast Ce^{3+} *d–f* emission is observed in both $SrCl_2$ and $BaCl_2$ under direct *f–d* excitation, host lattice (VUV) excitation and X-ray irradiation. The lifetime of the emission is 26 ns and 19 ns for Ce^{3+} in $SrCl_2$ and $BaCl_2$, respectively. After X-ray irradiation both Ce^{3+} activated compounds suffer from afterglow, which is most likely due to defect creation (e.g. color centers) by X-ray irradiation. The barium chloride results are in good agreement with the ones presented by Selling et al. [12], with the position of the cerium emission band being the same and where the afterglow has also been observed. Only the doublet structure of the cerium emission is not present in the spectra presented in this work, which might be related to the dose of the ionizing radiation used.

For Pr^{3+} in $SrCl_2$ and $BaCl_2$ fast *d–f* emission between 250 and 325 nm is observed under direct excitation into the *fd* states. The emission and excitation spectra show an about 12,180 cm^{-1} and 12,610 cm^{-1} shift to higher energies of the lowest *fd* state in comparison with the lowest 5*d* state for Ce^{3+} in the same host lattice for strontium chloride and barium chloride, respectively, in relatively good agreement with the expected shift based on the Dorenbos formula of 12,240 cm^{-1}. The lifetime of the Pr^{3+} *d–f* emission is about 13 ns in $SrCl_2$ and 10 ns in $BaCl_2$ which are among the fastest radiative decay times observed for *d–f* emission from lanthanide ions. Under host lattice excitation and X-ray irradiation no *d–f* emission

is observed. Instead, slow host lattice related emission bands are observed along with *f–f* emission. The absence of *d–f* emission is explained by the high energy positions of the *fd* excited states for Pr^{3+}. The *fd* states are at higher energies than the host lattice emissions of both $SrCl_2$ and $BaCl_2$ (situated between 300 and 500 nm) and as a result there is no energy transfer from the host lattice to the *fd* states of Pr^{3+} in $SrCl_2$ and $BaCl_2$. The absence of energy transfer from the host lattice to the Pr^{3+} *fd* states makes $SrCl_2$ and $BaCl_2$ doped with Pr^{3+} unsuitable for application as fast scintillator materials, in spite of the superior fast decay time in comparison to known Ce^{3+} and Pr^{3+} scintillator materials.

Emission spectra for $SrCl_2$ and $BaCl_2$ doped with Nd^{3+} under VUV and X-ray excitation show only intraconfigurational $4f^3$ emission lines and host lattice related emission bands. No evidence for *d–f* emission from Nd^{3+} was found. The absence for *d–f* emission, even upon direct excitation in the *fd* band, is explained by the high energy position of the $4f^2 5d$ levels of neodymium very close to or in the conduction band of $SrCl_2$ and $BaCl_2$.

Acknowledgements

The authors wish to acknowledge the financial support from the EU String project (NMP3-CT-2006-032636), as well as dr. A. Kotlov for help during the measurements at the Superlumi beam line at HASYLAB, DESY (Hamburg).

References

[1] W.W. Moses, Nucl. Instrum. Methods A 580 (2007) 919.
[2] G. Muehllehner, J.S. Karp, Phys. Med. Biol. 51 (2006) R117–R137.
[3] P. Dorenbos, J. Lumin. 91 (2000) 155.
[4] E. Zych, in: H. Singh Nalwa, L. Shea Rohwer (Eds.), Handbook of Luminescence Display Materials, and Devices, vol. 2, American Scientific Publishers, 2003, pp. 251–300.
[5] E.V.D. van Loef, P. Dorenbos, C.W.E. van Eijk, K.W. Krämer, H.U. Güdel, Nucl. Instrum. Methods A 486 (2002) 254.
[6] A. Bessiere, P. Dorenbos, C.W.E. van Eijk, K.W. Kramer, H.U. Güdel, C. de Mello Donegá, A. Meijerink, Nucl. Instrum. Methods A 537 (2005) 22.
[7] E.V.D. van Loef, P. Dorenbos, C.W.E. van Eijk, K.W. Kramer, H.U. Güdel, Nucl. Instrum. Methods A 496 (2003) 138.
[8] M.D. Birowosuto, P. Dorenbos, J.T.M. de Haas, C.W.E. van Eijk, K.W. Kramer, H.U. Güdel, J. Lumin. 118 (2006) 308.
[9] W. Drozdowski, A.J. Wojtowicz, Nucl. Instrum. Methods A 486 (2002) 412.
[10] J. Selling, S. Schweizer, M.D. Birowosuto, P. Dorenbos, IEEE Trans. Nucl. Sci. 55 (2008) 1183.
[11] J. Selling, Barium Halide Nanocrystals in Fluorozirconate based Glass Ceramics for Scintillation Application (PhD thesis, Universität Paderborn), 2007.
[12] J. Selling, S. Schweizer, M.D. Birowosuto, P. Dorenbos, J. Appl. Phys. 102 (2007) 074915.
[13] J. Selling, Ce-doped $BaCl_2$ and fluorochlorozirconate glass-ceramic X-ray storage phosphors (MSc thesis, Universität Paderborn) 2004.
[14] O.T. Antonyak, I.V. Kityk, N.S. Pydzyrailo, Opt. Spectrosk. 63 (1987) 529.
[15] O.T. Antonyak, I.V. Kityk, N.S. Pydzyrailo, Opt. Spectrosk. 69 (1990) 606.
[16] W.M. Li, M. Leskelä, Mater. Lett. 28 (1996) 491.
[17] A. Zych, C. de Mello Donegá, A. Meijerink, J. Lumin. 129 (2009) 1535.
[18] PDF (Powder Diffraction File) # 01-072-1537.
[19] PDF (Powder Diffraction File) # 01-072-1388.
[20] G. Zimmerer, Nucl. Instrum. Methods A 308 (1991) 178.
[21] Ch. Sugiura, Phys. Rev. B 9 (1974) 2679.
[22] K. Onodera, M. Koshimizu, K. Asai, Radiat. Phys. Chem. 78 (2009) 1031.
[23] J. Selling, M.D. Birowosuto, P. Dorenbos, S. Schweizer, J. Appl. Phys. 101 (2007) 034901.